

Bayesian Optimization of Crossbar-Based Compute-In-Memory System Design for Efficient DNN Inference

Arnob Saha¹, Bibhas Manna², Nikhil Kotikalapudi¹, Md Zesun Ahmed Mia¹, Rahul Kumar³, Madhavan Swaminathan¹, Abhronil Sengupta¹

¹ Penn State University, University Park, PA, USA, ² National Institute of Technology, Meghalaya, India, ³ Ansys, India

Abstract—Leveraging the high density and energy efficiency of Compute-In-Memory (CIM) crossbar-based Deep Neural Network (DNN) accelerators requires optimal Design Space Exploration (DSE), which becomes increasingly challenging as complex models for advanced AI workloads expand the highly non-convex design space. Moreover, heterogeneous layer workloads (e.g., memory- vs. compute-bound) and learning representations make layer-wise NN parameter allocation beneficial for efficiency but severely exacerbate the design space complexity by expanding the number of parameters to be tuned for simultaneous multi-objective optimization. Among existing DSE approaches, multi-objective Bayesian Optimization (BO) is promising, as it explores high-quality design solutions while querying costly CIM simulators selectively. In this work, we propose a multi-objective BO framework that holistically co-optimizes hardware and algorithm parameters of a CIM crossbar-based hardware accelerator for various DNN inference tasks. Depending on NN model depth, our framework handles high-dimensional design spaces (with 26 and 50 dimensions) and extremely large search complexities on the order of $O(10^{12})$ and $O(10^{27})$ for VGG8/CIFAR-10 and VGG16/Tiny-ImageNet-200. Our method attains 91.72% and 57.2% accuracy, respectively, comparable to baseline designs, while improving chip area (65.52% and 50.7%), read latency (9.52% and 13.27%), read dynamic energy (31.23% and 52.07%) and increasing memory utilization (13.41% and 2.67%).

Index Terms—Bayesian optimization, Multi-objective optimization, Design space exploration, CIM crossbar design, DNN inference

I. INTRODUCTION

Inspired by the human brain, artificial neural networks now power many real-world applications such as image recognition, speech understanding, and language processing. As these applications grow more complex and data-intensive, networks have scaled in depth and size, giving rise to Deep Neural Networks (DNNs). Nevertheless, limited computation, memory, and communication resources in edge processing environments make hardware implementation of DNNs challenging, as they must perform computationally expensive vector-matrix multiplications (VMMs) efficiently. In that regard, non-volatile memory (NVM) device-based CIM crossbar systems have shown superior performance over CMOS-based DNN hardware accelerators [1] [2] that suffer from the traditional von Neumann bottleneck [3] [4]. They also outperform SRAM-based CIM hardware accelerators in terms of density, multi-bit storage capability, and faster parallel computation

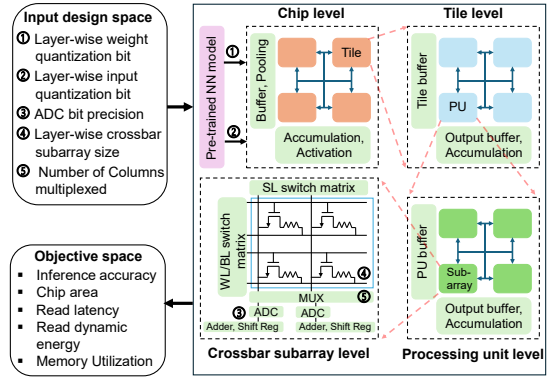


Fig. 1: Crossbar-based CIM system design hierarchy [6] and corresponding design space definitions.

[5]. Traditionally, a CIM crossbar system is organized in a hierarchy, as shown in Fig. 1, where the bottom-most crossbar subarray level is grouped into multiple processing units, which are in turn organized into multiple tiles, and all tiles are finally integrated at the chip level. Due to the analog nature of the crossbar inputs and outputs, each level requires associated Analog-to-Digital Converters (ADCs), input/output buffers, switching matrices, and other peripheral circuits, which collectively incur significant chip area, data processing time, and energy overhead. Therefore, accurately evaluating DNN inference performance on such hardware requires careful tuning of both algorithm- and hardware-level design parameters, including weight and input quantization bits, ADC resolution, crossbar subarray size, and others. Moreover, as different NN layers can have varying workload characteristics (memory-bound or compute-bound) [7], layer-wise parameter allocation is very useful for efficient hardware accelerator design compared to assigning identical parameter values across all NN layers that can lead to unnecessary area, latency, and energy overhead. The situation is further complicated by the fact that different DNN layers may carry varying levels of importance due to their learnt representations and therefore benefit from different design choices like weight and input bit precision [8]. Fig. 2 illustrates the algorithm- and hardware-level performance analysis—covering chip area, read latency, read dynamic energy, and memory utilization—for a VGG8/CIFAR-10 classification task under NN layer-wise and uniform allocations of the input design space parameters.

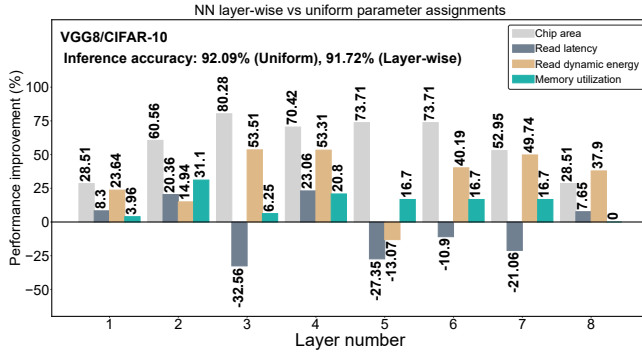


Fig. 2: Performance comparison between NN layer-wise and uniform parameter assignments.

Layer-wise parameter assignment can significantly improve overall hardware efficiency while maintaining approximately the same inference accuracy. Notably, it may not improve per layer performance for every objective, but it can yield better overall system-level performance with efficient techniques for design space exploration (DSE).

Nevertheless, layer-wise parameter assignment increases the dimensionality of the design space and the complexity of finding the best hardware accelerator configuration for a given NN model, especially for deeper networks and more complex datasets. In addition, different performance metrics are predominantly influenced by different design parameters, which often impose conflicting requirements. Consequently, it is crucial to obtain a single design that simultaneously improves all objectives, making the search for an optimal CIM crossbar system naturally formulated as a multi-objective optimization problem over multiple intertwined, and conflicting objectives. While there are multiple approaches to DNN hardware accelerator DSE, this problem space has been relatively underexplored for memristive CIM systems, primarily due to the fact that CIM hardware simulators are computationally expensive in terms of run-time and simplified functional abstractions are not valid at scale due to continuous data representation transfer between analog and digital domains. **We believe Bayesian Optimization (BO) is uniquely suited for this problem setup because it utilizes probabilistic surrogate models and efficient sampling techniques to find high-quality Pareto optimal designs with far fewer expensive CIM simulator accesses.**

Contributions: To the best of our knowledge, multi-objective BO has not been comprehensively explored for efficient CIM hardware accelerator design with large design spaces. This work adopts a multi-objective BO-based cheap surrogate modeling scheme for NN layer-specific DSE of a CIM crossbar-based hardware accelerator for efficient DNN inference performance analysis. Our main contributions are:

- **Multi-objective BO for CIM DSE:** Multi-objective BO has been employed to efficiently optimize a CIM crossbar-based hardware accelerator with large, complex NN layer-wise design spaces.
- **Layer-wise parameter optimization:** For a discrete, non-differentiable search space, NN layer-wise parameter optimization has been exploited to effectively handle high design space complexity ($O(10^{12})$ and $O(10^{27})$)

and dimensionality (26 and 50) for VGG8 and VGG16, respectively.

- **Scalability and modularity:** The proposed framework has a modular design and can be easily extended to accommodate additional device-circuit-system level design choices. We show scalability of our proposed approach by demonstrating results on the Tiny-Imagenet-200 dataset.
- **Hardware-level gains:** Compared to baseline designs, chip area, read latency, read dynamic energy and memory utilization are improved by more than 50%, 9%, 31% and 2.5%, respectively, for 2 different workloads, without significantly sacrificing inference accuracy.
- **Efficient simulator usage and Pareto quality:** Under an iso-computation budget, the proposed multi-objective BO framework outperforms NSGA-II in discovering better Pareto solutions while querying the costly CIM simulator only once per iteration.

II. LITERATURE REVIEWS

We review prior works in this domain from two perspectives: (1) optimization algorithms and (2) NN layer-wise DSE.

Firstly, we revisit methods for exploring the design space of NN hardware accelerators, including (i) gradient-based methods, (ii) evolutionary algorithm-based approaches, (iii) reinforcement learning (RL)-based methods, (iv) deep learning (DL) model-based approaches, (v) generative AI methods, and (vi) information-theoretic multi-objective optimization algorithms, among others. Gradient-based methods are well suited to differentiable search spaces because they scale well and have low computational cost for finding global optima. However, they have high memory requirements and require gradient estimation strategies for non-differentiable search spaces [9]. In contrast, gradient-free evolutionary algorithm-based models [9]–[12] can heuristically explore non-differentiable search spaces, but they require objective function evaluation for each candidate design via a costly simulator, leading to high computational cost. Furthermore, RL-based methods have been used for device–circuit–architecture co-exploration of CIM neural accelerators [13] and for exploring mixed-precision quantization in DNN inference accelerators [7], [14], where an RL agent is trained to iteratively learn a quantization policy. However, RL-based methods typically have relatively slow search speed and high computational cost [15]. On the other hand, DL model-based approaches [16], [17], after offline training on simulator-labeled data, directly map workload features to a single best accelerator configuration via one forward pass, avoiding iterative search. These methods, however, lack generalizability and have only been demonstrated for low-dimensional design spaces. Moreover, GAN-based [18] and diffusion-based [19] generative AI methods have been proposed to accelerate DSE of CMOS-based neural network accelerator designs by avoiding iterative interaction with the simulator during search. However, they require very large simulated datasets for offline training and may need retraining if the set of design knobs (or their discrete choices) changes. In addition, the optimization landscapes considered in such CMOS-based approaches are relatively simple and do not

include a costly simulator-in-the-loop, which is necessary for inference performance analysis of memristive CIM systems requiring continuous data conversion between analog and digital domains. On the contrary, Information-theoretic multi-objective optimization has been used to optimize memristor-based crossbars for DNN inference with added stochastic noise [20], but the design space dimensionality in that work is very limited. Beyond these methods, Bayesian optimization (BO) has emerged as an effective, gradient-free, sample-efficient technique for black-box optimization problems [21]. Nonetheless, only a few prior works [22], [23] have used BO for hardware–software co-design of CMOS-based DNN accelerators, and only for relatively small search spaces. Moreover, multi-objective BO has been applied for hyperparameter optimization of CIM-based neural network accelerator design [24], where neural architecture search is performed over a small design space and is therefore disjoint from the problem setup considered herein.

Secondly, we have examined the design specifications of hardware accelerators in several prior works that employ various hardware aware techniques, including quantization of weights and inputs [7], [13], [14], [25]–[28], quantization of ADC bit precision [29]–[31], variation of crossbar array size [28], [31], and the number of crossbar array columns multiplexed to share a common ADC [32]. However, very few prior works have explored the efficacy of jointly optimizing NN layer-wise quantization and crossbar design parameters to assess their impact on multiple intertwined hardware- and algorithm-level objective functions. In this context, a layer-specific dual-phase co-search of different input design parameters in a crossbar-based computing framework has been reported [32], although delay, accuracy, and energy are optimized in two separate phases under a pre-specified area constraint, and additional batchnorm adaptation is used to mitigate quantization noise due to reduced quantization bit-width.

In summary, the feasibility, problem formulation, algorithmic workflow and effectiveness of multi-objective BO for efficiently optimizing CIM hardware accelerator designs with highly complex, high-dimensional design spaces has not yet been explored.

III. CIM CROSSBAR SYSTEM DESIGN SPECIFICATIONS

To extensively understand the trade-off among multiple intertwined objectives and design an optimal CIM crossbar system, this work considers the following input design space parameters and objective space functions.

Input design space: Layer-wise weight bit precision (WBP) and layer-wise input bit precision (IBP) utilize different quantization values to represent the analog weight parameters and inputs of each NN layer, respectively, in the CIM crossbar design. This relates to the learnt importance of various layers of the network. Layer-wise crossbar subarray size (CSS) allows each NN layer to use different crossbar subarray sizes to optimize hardware metrics like memory utilization, depending on a particular layer’s compute/memory requirements. We consider ADC bit precision (ABP) and the number of crossbar

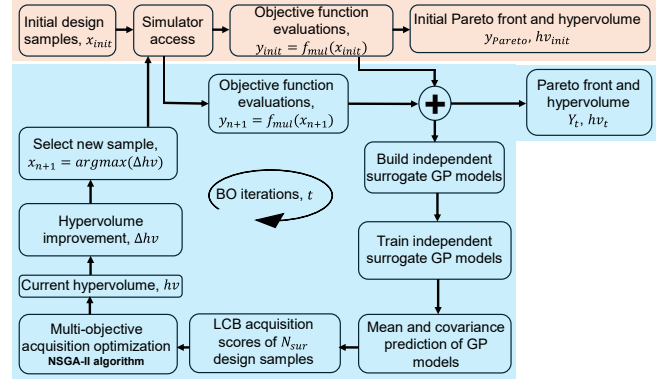


Fig. 3: Algorithmic flow of multi-objective BO.

subarray columns to be multiplexed for sharing one ADC (CCM) to be uniform across all layers and is chosen from a set of predefined values.

Objective space: In the proposed CIM crossbar system, DNN inference accuracy on different image recognition tasks is used as the algorithm-level performance metric, while chip area, read latency, read dynamic energy, and memory utilization are used as hardware-level metrics. It is noteworthy that read latency is defined as the time required to process a single image, and memory utilization is the ratio between the used memory and the total memory capacity [6]. The multi-objective BO framework aims to maximize inference accuracy and memory utilization while minimizing the other performance metrics.

IV. MULTI-OBJECTIVE OPTIMIZATION

A multi-objective optimization problem is defined as one with more than one objective function to be optimized. It can be formulated in vector form as,

$$f_{mul}(x) = [f^1(x), f^2(x), \dots, f^M(x)] \in \mathbb{R}^M, \quad M \geq 2, \quad (1)$$

where M is the number of objective functions and x denotes an input design with a predefined dimensionality. To identify all optimal design solutions, Pareto domination is used to compare objective vectors. Considering two different design solutions, x and x' , the objective vector $f_{mul}(x)$ Pareto dominates $f_{mul}(x')$ if $f^m(x) \geq f^m(x')$ for all $m = 1, 2, \dots, M$ and there exists at least one objective function f^m such that $f^m(x) > f^m(x')$. A design solution is classified as non-dominated if its objective vector is not dominated by any other objective vector in the set, and all such non-dominated vectors form the Pareto optimal front. The set of design solutions \mathbb{X} corresponding to the Pareto optimal front is called the Pareto optimal set [33].

V. BAYESIAN OPTIMIZATION ALGORITHM

Bayesian optimization (BO) is a model-based approach for solving optimization problems iteratively [34]. BO relies on a probabilistic surrogate model using Gaussian Process (GP) and an acquisition function which have been elaborately discussed in Section V-A and Section V-B, respectively. The surrogate model evaluates the efficacy of candidate design solutions in optimizing the objective functions, while the acquisition

function balances exploration and exploitation [35]. **The key advantage of utilizing the BO framework is the usage of the surrogate model for intelligently deciding on the next candidate solution (associated with costly CIM simulator access) to be added to the Pareto front.** The algorithmic flow of BO is illustrated step-by-step in Fig. 3 as follows,

Initialization: The optimization begins with passing a few initial design samples, x_{init} through the simulator to evaluate the corresponding objective vectors, y_{init} of the objective functions which are used to compute the initial Pareto front, y_{Pareto} and the initial hypervolume, $h_{v_{\text{init}}}$, a scalar metric measuring the volume of objective space dominated by a solution set and bounded by a reference point.

Surrogate model formulation: Gaussian surrogate models are then constructed for each objective, and the corresponding Gaussian likelihoods are defined.

Surrogate model training: The surrogate models are jointly trained by maximizing the marginal log-likelihood using the Adam optimizer.

Acquisition score calculation: At iteration, t , the predictive mean and variance of the surrogate models are computed for a set of N_{sur} new design samples and the corresponding acquisition scores are evaluated to form vector-valued acquisition functions, $\alpha = [\alpha_1, \alpha_2, \dots, \alpha_M]$, where each α_m corresponds to one objective. We use the acquisition function values as a proxy for the various objectives.

Multi-objective acquisition optimization: For the resulting discrete, multi-modal acquisition landscape, the derivative-free NSGA-II algorithm optimizes the acquisition function using Simulated Binary Crossover (SBX) and polynomial mutation [10], yielding the non-dominated Pareto front of acquisition values.

Hypervolume improvement evaluation: The non-dominated Pareto front of the acquisition values is combined with the Pareto front obtained in the previous iteration (y_{Pareto} for $t = 1$) to compute the current hypervolume, h_v . The hypervolume improvement, Δh_v over the previous iteration ($h_{v_{\text{init}}}$ for $t = 1$) is then evaluated.

New sample selection and surrogate model update: The design x_{n+1} yielding maximum Δh_v is selected and evaluated by the CIM simulator to obtain the new objective vector, y_{n+1} . The surrogate models are updated with this new sample, and the algorithm proceeds to the next BO iteration. At every iteration, the Pareto front, Y_t and hypervolume, h_{v_t} are evaluated which also represent the final outcomes after all iterations.

Thus, the BO-based optimization approach builds inexpensive surrogate models that are iteratively trained for efficient DSE of CIM systems associated with non-convex, discrete search space and costly-to-evaluate objective functions. To illustrate multi-objective BO, Fig. 4 provides a cartoon example of synchronously optimizing two objective functions over four iterations, t . Here, dotted red lines denote the target objective function values, and solid black lines denote the predicted values at each iteration. The confidence bounds, the acquisition scores for the two objective functions, and the minimum acquisition value used to select the next sample are represented by the gray regions, the blue-green inset plots, and

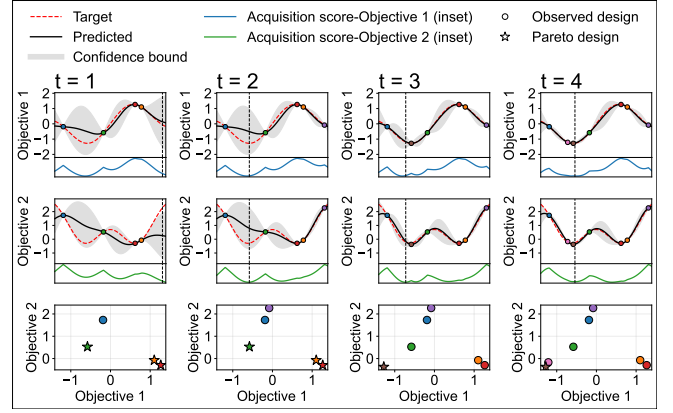


Fig. 4: Cartoon representation of optimizing 2 objective functions using multi-objective BO [36].

the vertical dotted black lines, respectively. The top and middle rows show objective values versus the input designs, and the bottom row shows the Pareto solutions of the two objectives. At each iteration, observed points and Pareto solutions are marked with circles and stars, respectively. Starting with four initial observations at $t = 1$, if an observed point is Pareto-efficient, its corresponding Pareto solution is indicated with a star of the same color in the bottom-left plot. As iterations proceed, the Pareto set evolves through efficient exploration of new observed points. However, this optimization becomes increasingly challenging as the number of objectives and the dimensionality of the design space grows.

A. Gaussian Process (GP) Model

GP is a popular model for BO as it provides closed-form predictions with quantified uncertainty and remains analytically tractable. Assume, $Y(x)$ is a GP model that can be defined by its prior mean function $\mu_0 : \mathcal{X} \in \mathbb{R}$ and covariance function $k : \mathcal{X} \times \mathcal{X} \in \mathbb{R}$ as [34] [37]:

$$Y(x) \sim GP(\mu_0, k) = \mathcal{N}(\mu_0, k) \quad (2)$$

$$\mu_0(x) = \mathbb{E}(Y(x)), x \in \mathcal{X} \quad (3)$$

$$k(x, x') = Cov(Y(x), Y(x')), (x, x') \in \mathcal{X}^2 \quad (4)$$

Here, x and x' are two different design candidates in the design space. Considering n number of design samples, the GP model can be written as a multivariate normal distribution:

$$Y(x_{1:n}) \sim \mathcal{N}(\mu(x_{1:n}), k(x_{1:n}, x_{1:n})) \quad (5)$$

Here, $\mu(x_{1:n})$ is the vector of $\mu_0(x_i)$ and $k(x_{1:n}, x_{1:n})$ is the matrix of $k(x_i, x_j)$, $1 \leq i, j \leq n$. To calculate the predicted mean and variance (useful for acquisition score calculation) at any new data point, $x_{\text{new}} \in N_{\text{sur}} \in \mathcal{X}$, the joint distribution of $Y(x_{1:n})$ and $Y(x_{\text{new}})$ can be expressed as:

$$\begin{pmatrix} Y(x_{1:n}) \\ Y(x_{\text{new}}) \end{pmatrix} \sim \mathcal{N} \left(\begin{pmatrix} \mu(x_{1:n}) \\ \mu(x_{\text{new}}) \end{pmatrix}, \begin{pmatrix} k(x_{1:n}, x_{1:n}) & k(x_{1:n}, x_{\text{new}}) \\ k(x_{\text{new}}, x_{1:n}) & k(x_{\text{new}}, x_{\text{new}}) \end{pmatrix} \right) \quad (6)$$

Thus, given $x_{1:n}$, addition of this new point results in another Gaussian process with mean, $\mu_n(x_{\text{new}})|_{x_{1:n}}$ that refers to the predicted objective function value at this point and variance,

TABLE I: Objective space performance comparison between NN layer-wise input design space parameter-assigned Pareto design and uniformly parameter-assigned designs for VGG8/CIFAR-10 task

Model: VGG8, Dataset: CIFAR-10										
Design	Input design space					Objective space				
	WBP	IBP	ABP	CSS	CCM	Accuracy (%)	Area (mm^2)	Latency (ms)	Energy (μJ)	Mem Util (%)
Variable WBP	3/4/5	5	5	256	8	91.48–92.09	7.1–10.5	0.59–0.76	9.55–15.18	62.92–83.89
Variable IBP	5	3/4/5	5	256	8	85.23–92.09	10.44–10.5	0.61–0.68	8.05–15.18	69.79
Variable ABP	5	5	4/5	256	8	80.47–92.09	10.4–10.5	0.61–0.63	8.97–15.18	69.79
Variable CSS	5	5	5	256/128/64	8	87.12–92.09	8.25–10.81	0.63–1.50	8.97–37.89	69.79–98.84
Variable CCM	5	5	5	256	16/8/4	92.09	10.5–10.7	0.52–0.92	14.53–16.51	69.79
Layer-wise BO	3/4/5	3/4/5	4/5	256/128/64	16/8/4	91.72	3.62	0.57	10.44	83.20

TABLE II: Objective space performance comparison between NN layer-wise input design space parameter-assigned Pareto design and uniformly parameter-assigned designs for VGG16/Tiny-ImageNet-200 task

Model: VGG16, Dataset: Tiny-ImageNet-200										
Design	Input design space					Objective space				
	WBP	IBP	ABP	CSS	CCM	Accuracy (%)	Area (mm^2)	Latency (ms)	Energy (μJ)	Mem Util (%)
Variable WBP	5/6/7/8	8	8	256	8	55–58.2	206.18–306.02	1.67–2.32	109.3–173	90.71–94.08
Variable IBP	8	5/6/7/8	8	256	8	51.3–58.1	306.02	1.55–2.32	117.66–173	94.08
Variable ABP	8	8	7/8	256	8	58.1	111.01–306.02	2.06–2.32	90.43–173	94.08
Variable CSS	8	8	8	256/128/64	8	58.1	306.02–862.23	2.32–13.75	173–304.43	94.08–99.89
Variable CCM	8	8	8	256	16/8/4	58.1	153.01–612.03	2.16–2.66	171.72–175.9	94.08
Layer-wise BO	5/6/7/8	5/6/7/8	7/8	256/128/64	16/8/4	57.2	136.61	1.83	72.3	95.03

$k_n(x_{new})|_{x_{1:n}}$ that determines the confidence of the prediction. In case of prediction with noisy observations having Gaussian noise of variance, λ^2 , $\mu_n(x_{new})|_{x_{1:n}}$ and $k_n(x_{new})|_{x_{1:n}}$ can be formulated as:

$$\mu_n(x_{new})|_{x_{1:n}} = \mu_0(x_{new}) + \mathbf{k}_{new}^T (K + \lambda^2 I)^{-1} (y_{1:n} - \mu(x_{1:n})) \quad (7)$$

$$k_n(x_{new})|_{x_{1:n}} = k(x_{new}, x_{new}) - \mathbf{k}_{new}^T (K + \lambda^2 I)^{-1} \mathbf{k}_{new} \quad (8)$$

where $\mathbf{k}_{new} = k(x_1, x_{new}), \dots, k(x_n, x_{new})$ is the covariance vector of $Y(x_{new})$ and $K = k(x_i, x_j), 1 \leq i, j \leq n$ is the covariance matrix of $Y(x_{1:n})$. $y_{1:n}$ defines the output vector of objective functions and I is an $n \times n$ identity matrix.

B. Acquisition Function

The acquisition function guides the search toward optimal solutions, with Expected Improvement (EI) and Probability of Improvement (PI) methods often becoming greedy when improvement is unlikely, while confidence-bound-based methods inherently balance exploration and exploitation. In confidence-bound methods, data points are chosen optimistically such that their objective values can serve as upper/lower bounds on the optimum [38]. While the Upper Confidence Bound (UCB) is typically used for maximization, the Lower Confidence Bound (LCB) [39] is its natural counterpart for minimization and both can be applied to the negated objective for minimization and maximization, respectively. This work primarily employs LCB for both minimization and maximization, with

$$\alpha_{LCB}(x_{new}, \beta) = \mu_n(x_{new}) - \beta \sigma_n(x_{new}), \quad (9)$$

where β is an appropriate constant, $\alpha_{LCB}(x_{new}, \beta)$ is the LCB acquisition function, $\mu_n(x_{new})$ is the GP predictive mean at x_{new} , and $\sigma_n(x_{new}) = \sqrt{k_n(x_{new})|_{x_{1:n}}}$ is the corresponding predictive uncertainty. For small β , LCB emphasizes exploitation in regions with low uncertainty, whereas larger β values encourage exploration in high-uncertainty regions [40].

VI. CROSSBAR BASED CIM SYSTEM PERFORMANCE BENCHMARKING

To benchmark algorithm- and hardware-level performance metrics of a crossbar-based CIM system design, NeuroSim [41], a popular architecture-level simulator, has been used as the black box function. In this work, VGG8, an 8 layer NN model (6 convolution and 2 linear layers), has been evaluated on CIFAR-10 dataset and VGG16, a 16 layer NN model (13 convolution and 3 linear layers), has been analyzed on Tiny-Imagenet-200 dataset. The models have been pre-trained using SGD optimizer for 200 iterations with initial learning rate of 0.01 and standard scheduler. As shown in Fig. 1, at every BO iteration, the simulator is launched with pre-trained analog weight values and layer-wise input design space parameters to evaluate the objective space functions. For layer-wise optimization, we considered different values for each input design parameter, as listed in Table I for VGG8/CIFAR-10 and in Table II for VGG16/Tiny-ImageNet-200. At every function query, each parameter can take any of these candidate values. These values are selected based on those reported in prior works [7], [25]–[30], [32]. Since we are focusing on inference operation, we limit the maximum bit precision for inputs and weights to 8 bits. For VGG16, higher WBP, IBP, and ABP are considered compared to VGG8 due to the complexity of the Tiny ImageNet dataset [42]. The training dataset is used for optimization and the resulting designs are validated on the test dataset to obtain the corresponding inference accuracy.

VII. RESULTS AND DISCUSSIONS

The efficacy of adopting multi-objective BO for designing a crossbar-based CIM system has been corroborated by analyzing 2 different image recognition tasks:

VGG8/CIFAR-10: For this 8-layer network, each design candidate has an input space dimensionality of 26, consisting of 8

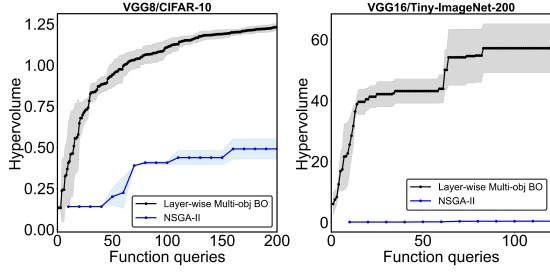


Fig. 5: Hypervolume comparison between multi-objective BO and NSGA-II.

layer-wise WBP, 8 layer-wise IBP, 8 layer-wise CSS, 1 ABP, and 1 CCM, whereas the objective space dimensionality is 5. According to the values of all input design space parameters, the design space complexity is on the order of $O(10^{12})$. The simulation has been performed for 200 BO iterations and surrogate GP models have been trained for 250 epochs at each iteration. Moreover, the best design sample has been selected from $N_{sur} = 2000$ design samples at every iteration. After finishing the repetitive process, 116 Pareto-optimal design solutions are obtained. Since inference accuracy is prioritized as the most critical objective, only 1 Pareto-optimal design having inference accuracy comparable to the uniformly parameter-assigned baseline design with the highest accuracy is selected for comparison. However, as illustrated in Table I, several uniformly parameter-assigned designs were configured, where each input design space parameter has been varied one at a time while the remaining parameters have been kept fixed at certain values and it is evident that more than one of these uniformly parameter-assigned designs achieve the highest accuracy. Therefore, the design configured with WBP of 5, IBP of 5, ABP of 5, CSS of 256, and CCM of 8 for all NN layers, is selected as the baseline. This baseline choice is motivated by the fact that while achieving highest accuracy, it consumes less area, and comparable latency and energy with respect to other uniformly parameter-assigned designs offering highest accuracy. The baseline design achieves 92.09% inference accuracy while consuming 10.5 mm² chip area, 0.63 ms read latency, 15.18 μ J read dynamic energy, and 69.79% memory utilization. In contrast, the selected layer-wise optimized Pareto design achieves 91.72% inference accuracy, degrading accuracy by only 0.37% compared to the baseline design, while improving chip area by 65.52%, read latency by 9.52%, read dynamic energy by 31.23%, and increasing memory utilization by 13.41%, as shown in Table I.

VGG16/Tiny-ImageNet-200: In this case, the input space dimensionality is 50, comprising 16 layer-wise WBP, 16 layer-wise IBP, 16 layer-wise CSS, 1 ABP, and 1 CCM and output space dimensionality is 5. Thus, with different values considered for each of the 50 input design space parameters, the DSE complexity becomes $O(10^{27})$. Following similar simulation process as discussed above for the other task, the optimization of such an expanded search space is conducted for 120 BO iterations on 1000 randomly selected training samples and later validated on 1000 randomly selected testing samples due to resource constraints. These subsets of the samples have been fixed for all the evaluations. The proposed

scheme attains 76 Pareto optimal design solutions during the optimization process, and among these, the Pareto optimal design with inference accuracy comparable to the baseline design is selected for comparison. As shown in Table II, among various designs obtained by following the same technique as the other task, the best design (58.2% inference accuracy) configured with (WBP=7, IBP=8, ABP=8, CSS=256, CCM=8) has been selected as baseline and it consumes 277.08 mm² chip area, 2.11 ms read latency, 150.84 μ J read dynamic energy, and achieves 92.36% memory utilization. Compared to the baseline design, the selected layer-wise optimized Pareto design achieves an inference accuracy of 57.2%, only 1% lower than the baseline, while improving chip area by 50.7%, read latency by 13.27%, read dynamic energy by 52.07%, and increasing memory utilization by 2.67%, as tabulated in Table II.

Moreover, Table I and Table II also show that the selected crossbar-based CIM system designs obtained by the proposed scheme outperform other designs with uniform parameter allocation across all NN layers in at least one or more objective function evaluations. Thus, the proposed multi-objective BO framework offers scalability and modularity, enabling its application to discrete and highly complex crossbar-based CIM system designs.

Simulator access and Pareto design quality: To evaluate the quality of the Pareto fronts obtained using the proposed multi-objective BO framework and to compare it with NSGA-II [12], a popular evolutionary algorithm, hypervolume indicator has been utilized. The hypervolume indicator measures how close a given approximation set is to the true Pareto front. It is commonly used for performance assessment and as a selection criterion in multi-objective optimization [43]. A higher hypervolume value indicates a higher quality Pareto solution. While, at every evolutionary iteration, NSGA-II must query the costly simulator multiple times to evaluate all design candidates—leading to slower processing and high computational cost, BO leverages probabilistic modeling and sampling strategies to intelligently select a single sample per iteration to pass through the costly simulator. This allows BO to perform many more iterations than NSGA-II under an iso-computation budget, thereby improving the quality of the Pareto designs. For illustration, the higher hypervolume values for multi-objective BO framework, plotted in Fig. 5, demonstrates the advantage of adopting the proposed approach over NSGA-II for optimizing crossbar-based CIM system designs under an equal number of function queries for the 2 different classification tasks with 1000 randomly selected training samples. The shaded regions refer to the standard deviation of 4 independent measurements and solid lines indicate the average hypervolume. It is to be noted that for complex models and datasets, NSGA-II struggles to improve the hypervolume over iterations.

VIII. CONCLUSIONS

This work leverages the sampling intelligence of multi-objective BO and the effectiveness of layer-wise parameter allocation to efficiently design complex crossbar-based CIM systems with optimized performance metrics. To the

best of our knowledge, this is the first extensive work on the feasibility analysis, problem formulation and quantitative evaluation in applying multi-objective BO to crossbar-based CIM hardware accelerator design. Future work can focus on accelerating optimization convergence for more complex models and datasets by exploring alternative multi-objective BO techniques. Investigation of DSE for CIM systems catered for Transformer architectures is also highly relevant.

ACKNOWLEDGMENTS

This material is based upon work supported primarily by the National Science Foundation under Grant No. CNS 2137259 - Center for Advanced Electronics through Machine Learning (CAEML) and its industry members.

REFERENCES

- [1] P. A. Merolla, J. V. Arthur, R. Alvarez-Icaza, A. S. Cassidy, J. Sawada, F. Akopyan, B. L. Jackson, N. Imam, C. Guo, Y. Nakamura *et al.*, “A million spiking-neuron integrated circuit with a scalable communication network and interface,” *Science*, vol. 345, no. 6197, pp. 668–673, 2014.
- [2] Y.-H. Chen, T. Krishna, J. S. Emer, and V. Sze, “Eyeriss: An energy-efficient reconfigurable accelerator for deep convolutional neural networks,” *IEEE journal of solid-state circuits*, vol. 52, no. 1, pp. 127–138, 2016.
- [3] I. Chakraborty, A. Jaiswal, A. Saha, S. Gupta, and K. Roy, “Pathways to efficient neuromorphic computing with non-volatile memory technologies,” *Applied Physics Reviews*, vol. 7, no. 2, 2020.
- [4] W. Haensch, A. Raghunathan, K. Roy, B. Chakrabarti, C. M. Phatak, C. Wang, and S. Guha, “Compute in-memory with non-volatile elements for neural networks: a review from a co-design perspective,” *Advanced Materials*, vol. 35, no. 37, p. 2204944, 2023.
- [5] S. Yu, “Neuro-inspired computing with emerging nonvolatile memories,” *Proceedings of the IEEE*, vol. 106, no. 2, pp. 260–285, 2018.
- [6] X. Peng, S. Huang, H. Jiang, A. Lu, and S. Yu, “Dnn+ neurosim v2. 0: An end-to-end benchmarking framework for compute-in-memory accelerators for on-chip training,” *IEEE Transactions on Computer-Aided Design of Integrated Circuits and Systems*, vol. 40, no. 11, pp. 2306–2319, 2020.
- [7] K. Wang, Z. Liu, Y. Lin, J. Lin, and S. Han, “Haq: Hardware-aware automated quantization with mixed precision,” in *Proceedings of the IEEE/CVF conference on computer vision and pattern recognition*, 2019, pp. 8612–8620.
- [8] I. Chakraborty, D. Roy, I. Garg, A. Ankit, and K. Roy, “Constructing energy-efficient mixed-precision neural networks through principal component analysis for edge intelligence,” *Nature Machine Intelligence*, vol. 2, no. 1, pp. 43–55, 2020.
- [9] H. Benmeziiane, K. E. Maghraoui, H. Ouarnoughi, S. Niar, M. Wistuba, and N. Wang, “A comprehensive survey on hardware-aware neural architecture search,” *arXiv preprint arXiv:2101.09336*, 2021.
- [10] Y. Lin, M. Yang, and S. Han, “Naas: Neural accelerator architecture search,” in *2021 58th ACM/IEEE Design Automation Conference (DAC)*. IEEE, 2021, pp. 1051–1056.
- [11] S.-C. Kao, M. Pellauer, A. Parashar, and T. Krishna, “Digamma: Domain-aware genetic algorithm for hw-mapping co-optimization for dnn accelerators,” in *2022 Design, Automation & Test in Europe Conference & Exhibition (DATE)*. IEEE, 2022, pp. 232–237.
- [12] K. Deb, A. Pratap, S. Agarwal, and T. Meyarivan, “A fast and elitist multiobjective genetic algorithm: Nsga-ii,” *IEEE transactions on evolutionary computation*, vol. 6, no. 2, pp. 182–197, 2002.
- [13] W. Jiang, Q. Lou, Z. Yan, L. Yang, J. Hu, X. S. Hu, and Y. Shi, “Device-circuit-architecture co-exploration for computing-in-memory neural accelerators,” *IEEE Transactions on Computers*, vol. 70, no. 4, pp. 595–605, 2020.
- [14] S. Huang, A. Ankit, P. Silveira, R. Antunes, S. R. Chalamalasetti, I. El Hajj, D. E. Kim, G. Aguiar, P. Bruel, S. Serebryakov *et al.*, “Mixed precision quantization for reram-based dnn inference accelerators,” in *Proceedings of the 26th Asia and South Pacific Design Automation Conference*, 2021, pp. 372–377.
- [15] O. Krestinskaya, M. E. Fouda, H. Benmeziiane, K. El Maghraoui, A. Sebastian, W. D. Lu, M. Lanza, H. Li, F. Kurdahi, S. A. Fahmy *et al.*, “Neural architecture search for in-memory computing-based deep learning accelerators,” *Nature Reviews Electrical Engineering*, vol. 1, no. 6, pp. 374–390, 2024.
- [16] A. Samajdar, J. M. Joseph, M. Denton, and T. Krishna, “Airchitect: Learning custom architecture design and mapping space,” *arXiv preprint arXiv:2108.08295*, 2021.
- [17] J. Seo, A. Ramachandran, Y.-C. Chuang, A. Itagi, and T. Krishna, “Airchitect v2: Learning the hardware accelerator design space through unified representations,” in *2025 Design, Automation & Test in Europe Conference (DATE)*. IEEE, 2025, pp. 1–7.
- [18] L. Feng, W. Liu, C. Guo, K. Tang, C. Zhuo, and Z. Wang, “Gandse: Generative adversarial network-based design space exploration for neural network accelerator design,” *ACM Transactions on Design Automation of Electronic Systems*, vol. 28, no. 3, pp. 1–20, 2023.
- [19] A. Ghosh, A. Moitra, A. Bhattacharjee, R. Yin, and P. Panda, “Diffaxe: Diffusion-driven hardware accelerator generation and design space exploration,” *arXiv preprint arXiv:2508.10303*, 2025.
- [20] X. Yang, S. Belakaria, B. K. Joardar, H. Yang, J. R. Doppa, P. P. Pande, K. Chakrabarty, and H. H. Li, “Multi-objective optimization of reram crossbars for robust dnn inferencing under stochastic noise,” in *2021 IEEE/ACM International Conference On Computer Aided Design (ICCAD)*. IEEE, 2021, pp. 1–9.
- [21] D. R. Jones, M. Schonlau, and W. J. Welch, “Efficient global optimization of expensive black-box functions,” *Journal of Global optimization*, vol. 13, no. 4, pp. 455–492, 1998.
- [22] Z. Shi, C. Sakhujia, M. Hashemi, K. Swersky, and C. Lin, “Using bayesian optimization for hardware/software co-design of neural accelerators,” in *Workshop on ML for Systems at the Conference on Neural Information Processing Systems (NeurIPS)*, 2020.
- [23] B. Reagen, J. M. Hernández-Lobato, R. Adolf, M. Gelbart, P. Whatmough, G.-Y. Wei, and D. Brooks, “A case for efficient accelerator design space exploration via bayesian optimization,” in *2017 IEEE/ACM International Symposium on Low Power Electronics and Design (ISLPED)*. IEEE, 2017, pp. 1–6.
- [24] M. Parsa, J. P. Mitchell, C. D. Schuman, R. M. Patton, T. E. Potok, and K. Roy, “Bayesian multi-objective hyperparameter optimization for accurate, fast, and efficient neural network accelerator design,” *Frontiers in neuroscience*, vol. 14, p. 667, 2020.
- [25] J. Bai, S. Sun, W. Zhao, and W. Kang, “Cimq: A hardware-efficient quantization framework for computing-in-memory-based neural network accelerators,” *IEEE Transactions on Computer-Aided Design of Integrated Circuits and Systems*, vol. 43, no. 1, pp. 189–202, 2023.
- [26] S. Huang, H. Jiang, and S. Yu, “Hardware-aware quantization/mapping strategies for compute-in-memory accelerators,” *ACM Transactions on Design Automation of Electronic Systems*, vol. 28, no. 3, pp. 1–23, 2023.
- [27] J.-W. Su, X. Si, Y.-C. Chou, T.-W. Chang, W.-H. Huang, Y.-N. Tu, R. Liu, P.-J. Lu, T.-W. Liu, J.-H. Wang *et al.*, “Two-way transpose multibit 6t sram computing-in-memory macro for inference-training ai edge chips,” *IEEE Journal of Solid-State Circuits*, vol. 57, no. 2, pp. 609–624, 2021.
- [28] F. Liu, W. Zhao, Z. Wang, Y. Zhao, T. Yang, Y. Chen, and L. Jiang, “Ivq: In-memory acceleration of dnn inference exploiting varied quantization,” *IEEE Transactions on Computer-Aided Design of Integrated Circuits and Systems*, vol. 41, no. 12, pp. 5313–5326, 2022.
- [29] H. Jiang, W. Li, S. Huang, S. Cosemans, F. Catthoor, and S. Yu, “Analog-to-digital converter design exploration for compute-in-memory accelerators,” *IEEE Design & Test*, vol. 39, no. 2, pp. 48–55, 2021.
- [30] T. P. Xiao, B. Feinberg, C. H. Bennett, V. Prabhakar, P. Saxena, V. Agrawal, S. Agarwal, and M. J. Marinella, “On the accuracy of analog neural network inference accelerators,” *IEEE Circuits and Systems Magazine*, vol. 22, no. 4, pp. 26–48, 2023.
- [31] S. Negi, I. Chakraborty, A. Ankit, and K. Roy, “Nax: neural architecture and memristive xbar based accelerator co-design,” in *Proceedings of the 59th ACM/IEEE Design Automation Conference*, 2022, pp. 451–456.
- [32] A. Moitra, A. Bhattacharjee, Y. Kim, and P. Panda, “Xpert: Peripheral circuit & neural architecture co-search for area and energy-efficient xbar-based computing,” in *2023 60th ACM/IEEE Design Automation Conference (DAC)*. IEEE, 2023, pp. 1–6.
- [33] L. Wang, A. H. Ng, and K. Deb, *Multi-objective evolutionary optimisation for product design and manufacturing*. Springer, 2011.
- [34] S. Zhang, S. Li, R. G. Harley, and T. G. Habetler, “An efficient multi-objective bayesian optimization approach for the automated analytical design of switched reluctance machines,” in *2018 IEEE Energy Conversion Congress and Exposition (ECCE)*. IEEE, 2018, pp. 4290–4295.

- [35] S. Daulton, D. Eriksson, M. Balandat, and E. Bakshy, "Multi-objective bayesian optimization over high-dimensional search spaces," in *Uncertainty in Artificial Intelligence*. PMLR, 2022, pp. 507–517.
- [36] E. Brochu, V. M. Cora, and N. De Freitas, "A tutorial on bayesian optimization of expensive cost functions, with application to active user modeling and hierarchical reinforcement learning," *arXiv preprint arXiv:1012.2599*, 2010.
- [37] C. K. Williams and C. E. Rasmussen, *Gaussian processes for machine learning*. MIT press Cambridge, MA, 2006, vol. 2, no. 3.
- [38] N. Srinivas, A. Krause, S. M. Kakade, and M. Seeger, "Gaussian process optimization in the bandit setting: No regret and experimental design," *arXiv preprint arXiv:0912.3995*, 2009.
- [39] K. Hanaoka, "Bayesian optimization for goal-oriented multi-objective inverse material design," *iscience*, vol. 24, no. 7, 2021.
- [40] S. Belakaria, A. Deshwal, N. K. Jayakodi, and J. R. Doppa, "Uncertainty-aware search framework for multi-objective bayesian optimization," in *Proceedings of the AAAI Conference on Artificial Intelligence*, vol. 34, no. 06, 2020, pp. 10 044–10 052.
- [41] X. Peng, S. Huang, Y. Luo, X. Sun, and S. Yu, "Dnn+ neurosim: An end-to-end benchmarking framework for compute-in-memory accelerators with versatile device technologies," in *2019 IEEE international electron devices meeting (IEDM)*. IEEE, 2019, pp. 32–5.
- [42] G. Charan, A. Mohanty, X. Du, G. Krishnan, R. V. Joshi, and Y. Cao, "Accurate inference with inaccurate rram devices: A joint algorithm-design solution," *IEEE Journal on Exploratory Solid-State Computational Devices and Circuits*, vol. 6, no. 1, pp. 27–35, 2020.
- [43] M. T. Emmerich, A. H. Deutz, and J. W. Klinkenberg, "Hypervolume-based expected improvement: Monotonicity properties and exact computation," in *2011 IEEE congress of evolutionary computation (CEC)*. IEEE, 2011, pp. 2147–2154.